Use of a simulation model and ecosystem flux data to examine carbon–water interactions in ponderosa pine

MATHEW WILLIAMS,[1,4] BEVERLY E. LAW,[2] PETER M. ANTHONI[3] and MICHAEL H. UNSWORTH[3]

[1] *The Ecosystems Center, Marine Biological Laboratory, Woods Hole, MA 02543, USA*

[2] *Department of Forest Science, Oregon State University, Corvallis, OR 97331, USA*

[3] *College of Oceanic and Atmospheric Sciences, Oregon State University, Corvallis, OR 97331, USA*

[4] *Present address: Institute of Ecology and Resource Management, University of Edinburgh, Darwin Building, Mayfield Rd., Edinburgh, EH9 3JU, U.K.*

Summary   Drought stress plays an important role in determining both the structure and function of forest ecosystems, because of the close association between the carbon (C) and hydrological cycles. We used a detailed model of the soil–plant–atmosphere continuum to investigate the links between carbon uptake and the hydrological cycle in a mature, open stand of ponderosa pine (*Pinus ponderosa* Dougl. *ex* Laws.) at the Metolius river in eastern Oregon over a 2-year period (1996–1997). The model was parameterized from local measurements of vegetation structure, soil properties and meteorology, and tested against independent measurements of ecosystem latent energy (LE) and carbon fluxes and soil water content. Although the 2 years had very different precipitation regimes, annual uptake of C and total transpiration were similar in both years, according to both direct observation and simulations. There were important differences in ratios of evaporation to transpiration, and in the patterns of water abstraction from the soil profile, depending on the frequency of summer storms. Simulations showed that, during periods of maximum water limitation in late summer, plants maintained a remarkably constant evapotranspirative flux because of deep rooting, whereas changes in rates of C accumulation were determined by interactions between atmospheric vapor pressure deficit and stomatal conductance. Sensitivity analyses with the model suggest a highly conservative allocation strategy in the vegetation, focused belowground on accessing a soil volume large enough to buffer summer droughts, and optimized to account for interannual variability in precipitation. The model suggests that increased allocation to leaf area would greatly increase productivity, but with the associated risk of greater soil water depletion and drought stress in some years. By constructing sparse canopies and deep rooting systems, these stands balance reduced productivity in the short term with risk avoidance over the long term.

Keywords: carbon cycle, drought, ecosystem model, Pinus ponderosa, rooting depth, transpiration, vapor pressure deficit.

Introduction

Global, regional and local hydrology are closely linked to the distribution and activity of vegetation (Eagleson 1978, Woodward 1987, Stephenson 1990). Because of the potential for changes in global climate, and thus patterns of precipitation (Houghton et al. 1996), understanding the links between hydrology and plant processes is of significant interest. Considerable efforts have been expended developing biogeographical and biogeochemical models to examine terrestrial ecosystem responses to global change (Melillo et al. 1995, Foley et al. 1998). However, the connections between weather and vegetation are poorly understood in detail, and are highly simplified in most models. There are relatively few studies or models that have characterised the dynamics of the soil–plant hydraulic pathway and explicitly linked liquid phase transport to vapor phase water losses from the canopy (Whitehead 1998). Thus, it is not clear to what degree the simple, semi-empirical relationships between soil water and vegetation processes that are commonly used in modeling exercises are adequate (Running and Coughlan 1988), or whether the details of the underlying mechanisms need to be incorporated (Williams et al. 1996).

The interactions between hydrology and plant processes are complicated because they occur at different scales and levels of organization. Both photosynthesis and transpiration at the leaf-level are dependent on local microclimate and coupled aerodynamic and stomatal conductances. But leaf-level demand for water must be matched by soil water abstraction by the whole plant, which is dependent on root distribution, soil water content, and hydraulic conductivity in the soil matrix (Hodnett et al. 1995, Dawson and Pate 1996, Williams et al. 1998). An excess of plant water use over recharge can induce restrictions on plant water uptake, reduce stomatal conductance, and cause a feedback on leaf-level processes and evaporative losses. Vegetation further affects soil water availability through the interception of precipitation (Gash 1979) and interactions with soil surface energy balance and evaporation.

We have previously developed a model of the soil–plant–atmosphere continuum (Williams et al. 1996), designed for testing against hourly time-series data from eddy covariance systems. The model is focused on canopy processes, and explores links between leaf-level water losses, leaf and soil water status, and liquid-phase fluxes from the soil through the plant. We hypothesized that plants regulate stomatal conductance to maximize C uptake while maintaining leaf water potential at or above a critical threshold that avoids cavitation. In tests in temperate deciduous forests (Williams et al. 1996), tropical rain forests (Williams et al. 1998), arctic tundra (Williams et al. 2000), and ponderosa pine (Law et al. 2000*b*), we were able to explain a large proportion of day-to-day variability in C exchange and latent energy (LE) fluxes, and the difference among sites, on the basis of a few key parameters and forcing variables. However, in the tropical study, we found that to explain seasonal variability in C and LE fluxes we had to invoke an increase in the resistance of the hydraulic pathway, associated with drier soils and reduced soil hydraulic conductivity during the dry season. Similarly, to explain activity during summer in the ponderosa pine study, soil water potential was required as a forcing variable. In both cases the original model formulation was unable to simulate and explore the interactions between plant and soil processes, specifically the feedbacks between soil water abstraction, hydraulic resistance and water potential gradients that the model-data comparison helped to identify. Another study with ponderosa pine (Law et al. 2000*a*) found that single-layer water balance models did not represent water use accurately, and recommended modeling multiple soil layers. Although simple empirical production models can be derived from measured productivity differences along a precipitation gradient (Runyon et al. 1994), they are not able to examine mechanisms of carbon–water interactions. Thus, the next stage of model development has been to incorporate an explicit multi-layer description of soil water dynamics and water abstraction of commensurate detail to the canopy model.

The goal of this study was to update, parameterize and test a linked model of ecosystem hydrology and primary production, and thus to determine the critical controls on carbon–water interactions in a drought-stressed forest ecosystem. We updated a process-based model of the soil–plant–atmosphere continuum (Williams et al. 1996) to incorporate a soil surface energy balance scheme, canopy interception of precipitation, coupled soil heat and water fluxes, and a spatially explicit 1-D root distribution. We then parameterized and tested the model using a detailed data set gathered over two years in a montane ponderosa pine forest in central Oregon (Law et al. 2000*b*), and examined how hydrological factors affected primary production in this drought-prone system. We used a series of analyses to quantify the sensitivity of this ecosystem to water stress, and investigated plant allocation patterns, especially below ground, in relation to drought stress.

Soil–plant–atmosphere model (SPA)

The soil–plant–atmosphere canopy model (SPA; see Williams et al. 1996 for a full description) is a multi-layer simulator of C_3 vascular plant processes. The model has 10 canopy layers and a 30-min time step, and ecosystem structure is described by vertical variations among canopy layers in light absorbing leaf area, photosynthetic capacity, and plant hydraulic properties. The model has a detailed radiative transfer scheme that calculates sunlit and shaded fractions of the foliage in each canopy layer (Williams et al. 1998). The maximum rate of carboxylation (V_{cmax}) and the maximum rate of electron transport (J_{max}) are determined from A/c_i curves, measurements of net assimilation rate and internal CO_2 concentration, derived from leaf-level gas exchange studies. Following Epron et al. (1995), these values are corrected to account for mesophyll resistance. The other parameters for the Farquhar model (mesophyll resistance, CO_2 compensation point, Michaelis-Menten and inhibition constants, temperature response parameters) are unchanged from previous model applications in temperate forests (Williams et al. 1996).

The model algorithms adjust stomatal conductance to balance atmospheric demand for water with rates of water uptake and supply from soils. Atmospheric demand is governed by the vapor pressure difference between leaf internal air spaces and the atmosphere, and vapor phase exchange (E) is determined by the Penman-Monteith equation. Water loss (E) is linked to changes in leaf water potential (Ψ_l), according to the water potential gradient between leaf and soil, liquid phase hydraulic resistances (both below ground, R_b, and in plant stems, R_p) and the capacitance (C) of the pathway that links soil to leaf. Stomatal conductance is varied to maintain E at a rate that prevents Ψ_l falling below a critical threshold value (Ψ_{lmin}), where cavitation of the hydraulic system may occur. Thus, once $\Psi_l = \Psi_{lmin}$, E is set so that $d\Psi_l/dt = 0$, where

$$\frac{d\Psi_l}{dt} = \frac{\Psi_s - \rho_w gh - E(R_b + R_p) - \Psi_l}{C(R_b + R_p)}. \tag{1}$$

The gravitational component of leaf water potential is determined by the density of water (ρ_w), acceleration due to gravity (g), and the height above the reference plane (h). The reduction in stomatal conductance, and the consequent decrease in A, is most pronounced where atmospheric saturation deficit and plant hydraulic resistance are highest, usually in the upper canopy. We assume that plant hydraulic resistance (R_p) of each canopy layer increases with path-length, and so is determined from stem hydraulic conductivity (G_p, mmol m^{-1} s^{-1} MPa^{-1}), height of the layer (h, m), and leaf area of the layer (L, m^2 m^{-2}).

$$R_p = \frac{h}{G_p L}. \tag{2}$$

We have updated the SPA model to simulate soil surface energy balance, soil heat and water transport, root distribution

and water uptake, and the interception and evaporation of water on canopy surfaces.

Soil surface energy balance

The canopy radiative transfer scheme determines the downwelling radiation at the soil surface. We use this to solve the surface energy balance, by using a bisection method to find the soil surface temperature (T_{sur}) that balances net radiation (Q_{net}, determined from down-welling radiation and long-wave losses from the soil surface) with sensible (Q_h), latent (Q_e) and ground heat fluxes (Q_c), following the approach of Hinzman et al. (1998):

$$Q_h + Q_e + Q_{net} + Q_c = 0 \qquad (\text{W m}^{-2}). \qquad (3)$$

Calculation of the various components is described in the Appendix. For calculation of soil evaporation (Q_e), the model keeps track of multiple wetted layers that can develop with successive drying and wetting, merging layers that overlap. We found that without this detailed accounting, the match between predicted soil evaporation and measured fluxes was poor during summer, when heavy storms alternate with periods of low atmospheric humidity.

Soil heat and water transport

The soil is divided into layers of constant thickness, of a given organic matter and mineral content. The flux of heat through the soil profile is determined on the basis of the ground heat flux, Q_h, the thermal gradient between soil layers, the soil thermal conductivity (k) and thermal heat content of each layer (c_v, the soil volumetric heat capacity), by the Fourier heat conduction equation:

$$\frac{\partial T}{\partial t} = \frac{\partial}{\partial z}\left(\frac{k}{c_v}\frac{\partial T}{\partial z}\right). \qquad (4)$$

The thermal parameters are dependent on soil organic matter and mineral fractions and soil water content (Hillel 1980), and phase transitions between liquid water and ice (Waelbroeck 1993). The Fourier equation is solved implicitly by the Crank-Nicholson scheme (Farlow 1993).

The porosity and soil water retention curves of each layer are estimated according to empirical relationships with soil texture (Saxton et al. 1986). Changes to layer water content are regulated by precipitation and evaporation (surface layer only), abstraction by roots (rooted layers only), and gravitational drainage. Heavy snowfall is uncommon at the study site, and there is no detailed snow model; below-freezing precipitation is stored and only added to the upper soil layer when temperatures rise above freezing. Infiltration rates are assumed to be greater than precipitation rates, and surface runoff occurs only when the water content of the surface layer exceeds porosity. Gravitational drainage occurs when water content is above a set fraction of porosity; the rate of drainage is set directly by the soil hydraulic conductivity (m s^{-1}), another function of texture and water content (Saxton et al. 1986). The

discharge from the soil profile is determined as the flux of water crossing the lower boundary of the soil profile by gravitational drainage. Heat is redistributed through the soil profile according to water movement. From patterns of freezing and thawing, the ice content of each soil layer is determined by linear interpolation.

Root distribution and water uptake

Plant root distribution is determined by total fine root biomass (F_{total}, g m^{-2}), maximum root biomass per unit volume (F_{max}, g m^{-3}), which is assumed to occur at the soil surface, and depth of rooting (D_{max}, m). Assuming an exponential decay in root length with depth, root biomass per unit volume (F, g m^{-3}) at any depth is given by:

$$F = F_{max}e^{-\kappa D}, \qquad (5)$$

where coefficient κ is linked to the other parameters by:

$$F_{total} = F_{max}\int_0^{D_{max}}e^{-\kappa D}dD. \qquad (6)$$

This equation can be rearranged and κ determined numerically.

Belowground hydraulic resistance has a soil component (R_s) and a root component (R_r). The soil component is dependent on soil conductivity (G_{soil}, mmol m^{-1} s^{-1} MPa^{-1}, a function of soil water content and texture), fine root radius (r_r, m), root length per unit soil volume (l_R, determined from biomass and radius), depth of the soil layer (D, m) and mean distance between roots (r_s, m, $(1/(\pi l_R D))^{0.5}$) (Newman 1969):

$$R_s = \frac{\ln(r_s/r_r)}{2\pi l_R D G_{soil}}. \qquad (7)$$

Root hydraulic resistance for each rooted soil layer declines linearly with increasing root biomass according to root resistivity R_r^* (MPa s g mmol^{-1}):

$$R_r = R_r^*/(FD). \qquad (8)$$

The relative contribution of roots in each soil layer to total root activity is determined from the maximum potential water uptake (E_{max}) of each soil layer. According to Equation 1, once the minimum leaf water potential has been reached, the sustainable flux rate is determined by the difference between soil water potential (Ψ_s) and minimum sustainable leaf water potential (Ψ_{lmin}), and hydraulic resistance of soil and roots in each soil layer;

$$E_{max} = \frac{\Psi_s - \Psi_{lmin}}{R_s + R_r}. \qquad (9)$$

From the estimate of E_{max} for each of the l soils layers with roots, we determine a weighted soil water potential (Ψ_{sw}), which is applied in Equation 1:

$$\Psi_{sW} = \frac{\sum_{i=1}^{l}(\Psi_{si}E_{\max i})}{\sum_{i=1}^{l}(E_{\max i})}. \tag{10}$$

For each canopy layer i, the total root and soil hydraulic resistance (R_{bi}) is determined by assuming that each such layer is connected to each soil layer; i.e., the roots in each soil layer supply a fraction of the water to each canopy layer. We assume that the fraction of roots in each root layer supplying each canopy layer is the same as the ratio of leaf area in the canopy layer (L_i) to total leaf area (L_{tot}):

$$R_{bi} = \frac{1}{\sum_{j=1}^{l}\left(\frac{(R_{sj}+R_{rj})L_{tot}}{L_i}\right)}. \tag{11}$$

The total amount of water extracted by roots from the soil in each time-step is determined by Equation 1 and split between rooted layers according to the weighting $E_{\max i}/\Sigma(E_{\max})$.

Interception and evaporation on canopy surfaces

Precipitation inputs to soils are calculated after canopy interception, drainage and evaporation from the canopy water store, following the approach of Rutter et al. (1975). The canopy is regarded as having a surface storage capacity S that is charged by rainfall and discharged by evaporation and drainage. The through-fall parameter determines what fraction of precipitation reaches the soil surface directly; the remainder is added to the canopy store. When the amount of water on the canopy equals or exceeds S, then evaporation (E) is determined by the Penman-Monteith equation, with stomatal resistance set to zero. When storage s is less than capacity S, then evaporation occurs at a rate $E(s/S)$. The rate of drainage from the canopy (d, mm h^{-1}) is given by:

$$d = \exp(a+bs), \tag{12}$$

where a and b are empirically derived constants. A Runge-Kutta integrator (Press et al. 1986) determines the total drainage and evaporation during each model time-step (30 min).

Study area

The Metolius ponderosa pine site is located in a Research Natural Area (44°30′ N, 121°37′ W, elevation 940 m) in the eastern Cascades, near Sisters, Oregon (Anthoni et al. 1999). The stand consists of old (~250 years), young (~45 years) and mixed old and young patches of ponderosa pine. The canopy reaches a maximum height of about 43 m, and is relatively open. The understory vegetation is sparse with patches of bitterbrush (*Purshia tridentata* (Pursh) DC.) and bracken fern (*Pteridium aquilinum* (L.) Kuhn), and a groundcover of strawberry (*Fragaria vesca* L.).

The site experiences warm dry summers and cool wet winters. Total precipitation in 1996 was 869 mm, a wetter than normal year, and 488 mm in 1997. Mean annual temperature was 8.4 °C in 1996 and 8.5 °C in 1997. Total irradiance was 5390 MJ m^{-2} in 1996 and 5355 MJ m^{-2} in 1997. Soil texture analysis indicated that the soil is 73% sand, 21% silt, and 6% clay. The sandy loam soils are low in nutrients.

Environmental measurements

We made continuous eddy covariance measurements to determine half-hourly fluxes of CO_2 and water vapor above and below the forest canopy in 1996 and 1997. The instruments were positioned on a tower at 47 m, and at 2 m above the soil surface. Full details of the instrumentation and flux corrections are reported in Law et al. (1999*a*, 1999*b*) and Anthoni et al. (1999). Data were screened to remove possible eddy covariance instrumentation and sampling problems (Law et al. 1999*b*). Fluxes were also rejected when unreasonably large CO_2 fluxes ($|F_c| > 25$ µmol m^{-2} s^{-1}) were observed. After screening, about 75% of the above-canopy carbon flux and 85% of the water vapor fluxes remained available for further analysis.

Meteorological variables were calculated as half-hourly means from measurements made at the top of the tower (air temperature, vapor pressure deficit, precipitation, diffuse and direct photosynthetically active radiation (PAR), global solar radiation, net radiation). Soil water content was measured at 0–0.3 m depth in several locations by automated and manual time domain reflectometry (Campbell Scientific, Logan, UT; Tektronix, Beaverton, OR).

Ecological measurements

We measured assimilation rates in relation to leaf internal CO_2 repeatedly (Law et al. 1999*b*), to provide the models with estimates of maximum carboxylation (V_{cmax}) and electron transport rates (J_{max}). Other periodic gas exchange measurements included foliage and stem respiration, and soil surface CO_2 fluxes for estimating hourly ecosystem respiration (R_e) from the meteorological data (Law et al. 1999*b*).

We estimated leaf area index (one-sided LAI) from optical measurements at 5 m intervals over a 10,000 m^2 plot with an LAI-2000 plant canopy analyzer (PCA; Li-Cor, Lincoln, NE). We also measured needle clumping within shoot, and clumping at scales larger than shoot (Law et al., unpublished data) to correct for these effects on LAI estimates. The seasonal change in LAI was calculated from the fractional change in monthly litterfall and the optical estimates of summer maximum LAI. Understory LAI was estimated by the line intercept method within a 1×1 m frame at 13 locations (Law et al. 1999*b*). Because most of the understory was *Fragaria vesca* (flat, planofile leaves), LAI was estimated to be the same as the percentage cover. Total LAI varied between a minimum of 1.1 and a maximum of 1.6.

Predictions of annual ecosystem water, energy and carbon exchange

We predicted exchanges of energy and water, and the fixation of C, at 30-min resolution over two full annual cycles (Ta-

ble 1). The model was forced with time-varying input variables, comprising 30-min meteorological data (temperature, vapor pressure deficit, irradiance, precipitation) and daily estimates of LAI and foliar nitrogen derived from measurements (ranges are shown in Table 2; peak values occur July–September). The remaining model parameters were constants, derived from measurements at the site (Table 2); in those cases where data were unavailable, the parameter was estimated, and subjected to scrutiny in a sensitivity analysis. In the case of canopy interception of precipitation, parameters from a Corsican pine stand were used (Rutter et al. 1975). The only root data available at the site were the biomass of fine roots in the surface 0.2 m (Table 2). From an inspection of tip-up mounds at the site we estimated rooting depth at 1.5 m, though some root balls did reach considerably deeper (up to 5 m). Lacking information on root distribution with depth, we set a total root biomass so that the root biomass per volume in the topmost layer was one order of magnitude larger than in the lowest rooted

layer. Root resistivity and stem conductivity were estimated from literature values (Tyree and Ewers 1996) (Table 2). The gravitationally retained fraction of total soil porosity was estimated at 60% from soil water content data collected during the early months of 1997. We used 20 soil layers each of 0.1-m thickness.

Comparison with eddy flux data

When a single parameterization was used, predicted latent energy fluxes were generally in close agreement with measured fluxes in both years (Figures 1 and 2). In 1996, the largest measured latent energy fluxes were recorded on a few days in the spring and fall, and these were not satisfactorily explained by the simulation. An analysis of these discrepancies revealed that precipitation occurred either on the day in question, or the previous day, in all but one case. When these days were removed from the analysis, the model explained 67% of daily variance in LE (Table 3). Most of the variability was related to changes in daily incident radiation; statistical regression indicated that radiation could explain 57% of the variability in non-rain day LE fluxes. In 1997, measured LE fluxes peaked during the summer, and simulated fluxes were in close agreement with measurements (Figure 2). The simulations explained 63% of daily variance (Table 3); linear statistical regression indicated that irradiance alone explained 59%.

We compared predicted GPP with estimates derived from measurements of whole-ecosystem NEP by eddy covariance, and of ecosystem respiration derived from soil, leaf and stem chamber data. The SPA model predictions in 1996 explained

Table 1. Predictions of gross primary production (GPP) and latent energy (LE) fluxes for the Metolius site, Oregon, in 1996 and 1997. Empirical equations were used to fill gaps in measurement data to produce annual measured estimates.

Year	GPP (g C m^{-2} year^{-1})		LE (mm year^{-1})	
	Measured	Modeled	Measured	Modeled
1996	1208 ± 184	1257	436 ± 65	346
1997	1262 ± 195	1287	400 ± 60	401

Table 2. Parameters of the soil–plant–atmosphere model.

Parameters	Units	Source	Value
Minimum leaf water potential (Ψ_{lmin})	MPa	Pressure chamber, this study	−2.0
Stem specific hydraulic conductivity (G_p)	mmol m^{-1} s^{-1} MPa^{-1}	(Tyree and Ewers 1996)	20.0
RuBP carboxylation catalytic rate coefficient at 30 °C	μmol g^{-1} N s^{-1}	A/C_i curve, this study	37.8
Electron transport rate coefficient at 30 °C	μmol g^{-1} N s^{-1}	A/C_i curve, this study	49.0
Through-fall fraction (unintercepted precipitation)	mm mm^{-1}	(Rutter et al. 1975)	0.7
Field capacity as fraction of total porosity		Estimated	0.6
Canopy surface water storage capacity (S)	mm	(Rutter et al. 1975)	1.0
Surface storage drainage parameter a	mm min^{-1}	(Rutter et al. 1975)	−9.9
Surface storage drainage parameter b	min^{-1}	(Rutter et al. 1975)	3.7
Maximum root biomass per volume (F_{max})	g m^{-3}	This study	1680
Total fine root biomass (F_{total})	g m^{-2}	Estimated	1000
Rooting depth	m	Estimated	1.5
Fine root radius (r_r)	m	Estimated	0.0005
Root resistivity (R_r*)	MPa s g mmol^{-1}	Estimated	400
Soil clay content	%	This study	6
Soil sand content	%	This study	73
Soil hydraulic conductivity (G_{soil})	mmol m^{-1} s^{-1} MPa^{-1}	Empirical	(Saxton et al. 1986)
Soil tortuosity		(Choudhury and Monteith 1988)	2.5
Thickness of soil layer (D)	m	N/A	0.1
Soil thermal conductivity (k)	J s^{-1} m^{-1} K^{-1}	(Hillel 1998)	See footnote
Soil volumetric heat capacity (c_v)	J m^{-3} K^{-1}	(Hillel 1998)	See footnote
Foliar N concentration	g N m^{-2} leaf area	This study	3.8–4.3
Leaf area index (LAI)	m^2 m^{-2}	This study	1.1–1.6

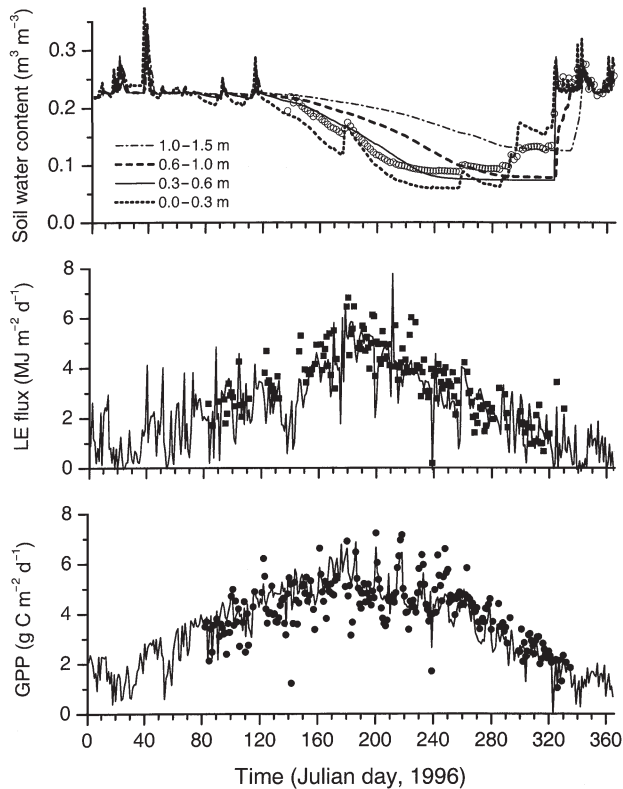[1] Functions of soil water, mineral, and organic matter content.

Figure 1. Time series of soil water content, latent energy (LE) flux, and gross primary production (GPP), both measured (symbols) and modeled (lines) in a ponderosa pine stand at Metolius, Oregon, in 1996. Latent energy fluxes are shown only for days without precipitation. The measured soil water content was at 0–0.3-m depth.
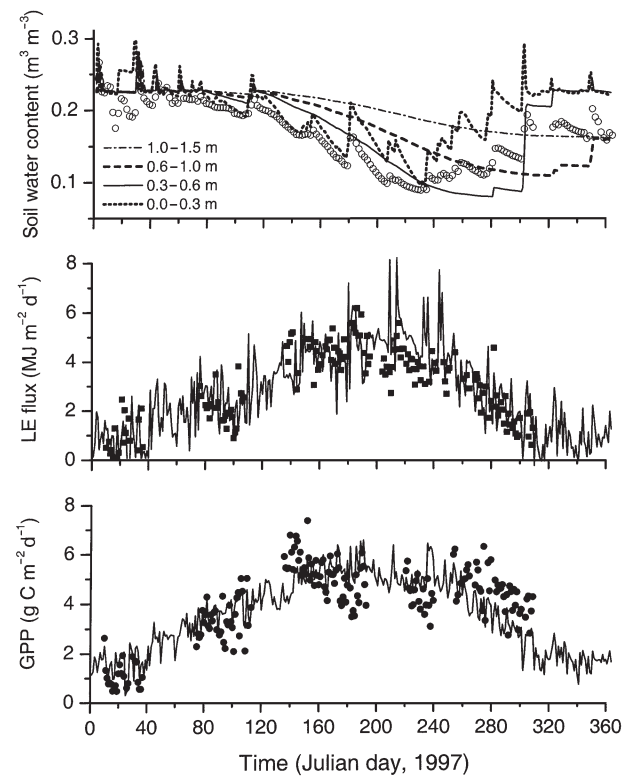

Figure 2. Time series of soil water content, latent energy (LE) flux, and gross primary production (GPP), both measured (symbols) and modeled (lines) in a ponderosa pine stand at Metolius, Oregon, in 1997. The measured soil water content was at 0–0.3-m depth.

66% of observed daily variance (Table 3), although simulations did not account for the extremes of productivity measured during the summer (Figure 1). Daily irradiance was a poor predictor of GPP, explaining only 35% of daily variability. The peaks and troughs of GPP predicted in SPA during late summer, which closely matched the patterns observed in the data (Figure 1), were induced by stomatal responses to atmospheric humidity, with significant reductions in conductance during high VPD days (> 3 kPa). In 1997, the model explained 65 % of daily variance in GPP (Table 3). The major discrepancies occurred in the autumn, when predicted uptake was less than observed uptake. Variation in daily irradiance explained only 32% of observed variance in GPP.

During portions of 1997, an eddy covariance system set up 2 m below the pine canopy provided measurements of energy exchange between the soil surface and the atmosphere. We compared the observed LE fluxes at this height with predicted Q_e from our soil surface energy balance routine. Over a 30-day period in August, the model explained both the background rate of evaporation during the initial dry days, and the rates following precipitation, subsequent drying, and further precipitation (Figure 3).

Comparison with soil water data

We compared predictions of soil water dynamics with daily observations of soil water at a depth of 0.0–0.3 m (Figures 1 and 2). In 1996, simulations suggested that soil water content

Table 3. Statistical comparison of modelled (abscissa) versus measured (ordinate) data, including slope and intercept of linear regression, and r^2. Abbreviation: SE = standard error of prediction. The LE regression does not include rain days (see text).

Comparison	Year	Number of data (n)	Slope of linear regression (SE)	Intercept of linear regression (SE)	r^2
GPP	1996	219	0.80 (0.04)	0.86 (0.17)	0.66
	1997	149	0.67 (0.04)	1.23 (0.17)	0.65
Latent energy	1996	165	0.76 (0.04)	0.53 (0.15)	0.67
	1997	158	0.71 (0.04)	0.66 (0.16)	0.63

generally declined smoothly from early summer onward, with abstraction gradually developing in successively deeper layers. The trajectory of measured water content matched that of simulated upper soil layers, with two clear exceptions: the initial decline in water content started later than in the simulation, and, in the autumn, the rate of soil recharge was slower than expected.

In 1997, there was close agreement in timing between simulated and recorded draw down in spring (Figure 2). Water content of the soil surface layer was frequently recharged by summer storms, and from mid-August (Day 230) onward, simulations suggested that the surface soil frequently had a higher water content by volume than the layers beneath it. However, measurements of soil water content were less responsive to these summer recharge events than the model suggested (Figure 2).

The predicted rate of water uptake from a particular soil depth depended on root biomass, soil water content and soil hydraulic conductivity in the corresponding soil layer. During winter, simulations suggested that freezing conditions in the surface soil redirected water withdrawal deeper in the profile (Figure 4); evapotranspiration was recorded and simulated even on days with mean temperatures of ~0 °C, in early 1997 (Figure 2). By spring, with thawed soils and increasing atmospheric demand, simulated uptake was concentrated in the most densely rooted surface layers. Then, during the summer of 1996, water was increasingly withdrawn from lower layers of the soil profile as surface layers dried out (Figure 1). By early September 1996 (Day 280), the simulations suggested that over 80% of water extraction by roots occurred below 0.8 m. Heavy rains then recharged the upper layers and uptake shifted higher in the soil profile. In 1997, the more even distribution of rain over the summer (Figure 5) meant that predicted water withdrawal was concentrated in the upper soil layers through most the year (Figure 4).

Predicted water fluxes

Predicted total canopy transpiration in 1996 (251 mm) and

Figure 4. Predicted fractions of total daily water uptake by roots from four soil depths, for 1996 (top) and 1997 (bottom).

1997 (265 mm) were almost identical (Figure 5). However, predictions of direct evaporation from the soil surface varied between years; predictions were 48% greater in 1997, because of summer precipitation. Similarly, the evaporation of water from the wetted canopy surfaces was 75% greater in 1997. The analysis suggests that the greatest hydrological difference between the 2 years was in the rates of discharge from the soil profile, and this was closely tied to the rates of winter precipitation (Figure 5).

Sensitivity and error analysis

We undertook a series of analyses to test the sensitivity of predictions to variation in the key parameters. We selected for analysis those parameters with the greatest uncertainty, often because of a lack of detailed site-specific data. These included through-fall fraction, total root biomass, depth of rooting, canopy surface water storage (S), root hydraulic resistivity, and gravitationally retained water as a fraction of soil porosity (field capacity). We also selected critical parameters in overall water balance, including LAI, total precipitation, minimum leaf water potential, soil texture, and surface rooting biomass.

We varied each of these 11 parameters individually, with the actual magnitude of variation applied in each case dependent on an estimation of natural variability in the parameter, or
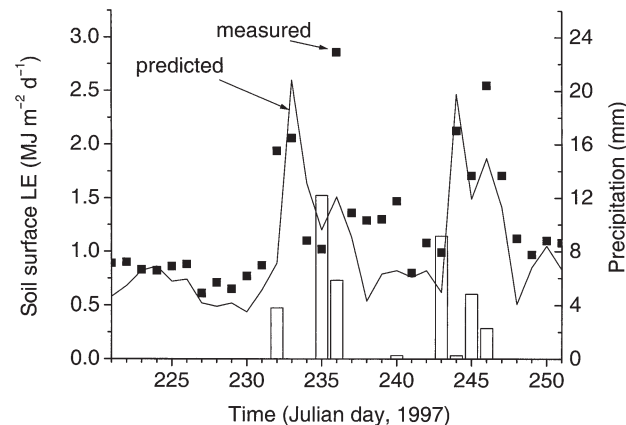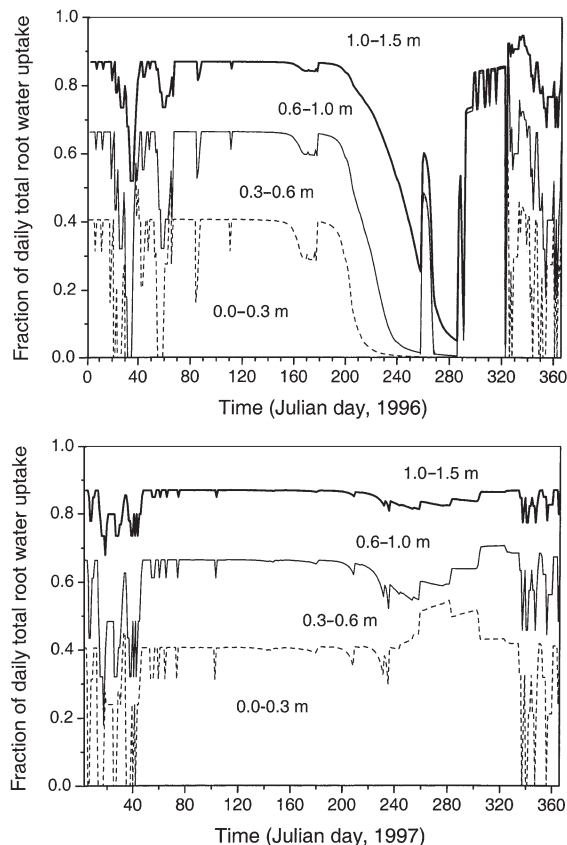

Figure 3. Time series of measured (symbols) and simulated (line) soil latent energy (LE) flux (left axis), and total daily precipitation (columns, right axis) during summer 1997 at the Metolius site.
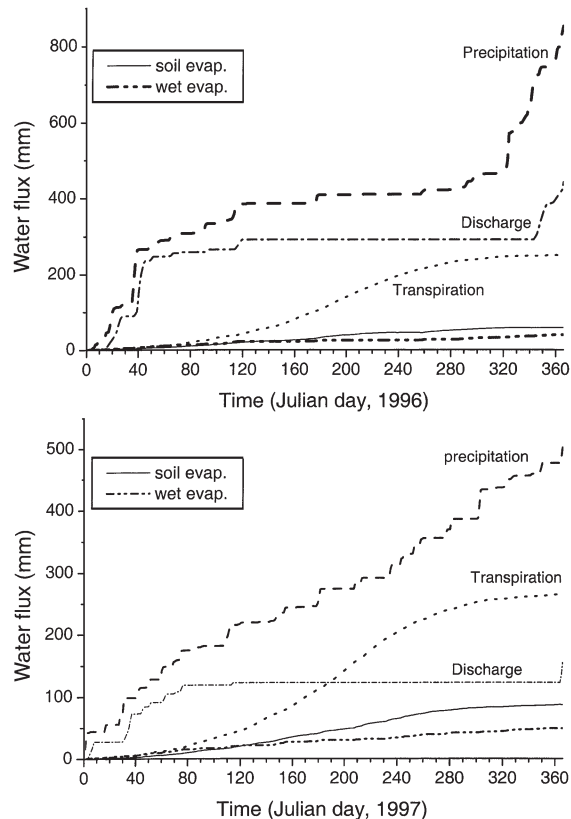
Figure 5. Cumulative water fluxes over 1996 (top) and 1997 (bottom). Precipitation was measured at the site, whereas soil evaporation, canopy evapotranspiration, evaporation from wetted canopy surfaces, and discharge from the soil profile were all simulated. Note the different scales on the two panels.

the degree of certainty in parameter assignment (Figure 6). For example, lacking any detailed data on root resistivity, we varied this parameter from 25 to 200% of the originally assigned value. Total root biomass was varied from 50 to 200% of the original estimate. For parameters that were better constrained by data, narrower ranges were selected; thus, precipitation was varied from 50 to 150% of measured values, and minimum leaf water potential from 75 to 125% of measured values.

We simulated a full year of interactive hydrology and production for each new parameter set, and examined the effect on annual GPP and total LE fluxes. We undertook the analyses twice; once using 1996 weather, and once using 1997 weather, to examine sensitivity to differences in precipitation patterns. The sensitivities of GPP and LE fluxes were similar in form (Figure 6), though not always in magnitude; we present results from 1996.

Carbon uptake and latent energy fluxes were most sensitive to changes in LAI (Figures 6a and 6d), which included an associated change in total foliar N. Doubling LAI raised annual GPP by 49% and LE by 19%, whereas a reduction in LAI by 50% reduced GPP by 38% and LE by 20%. Field measurements of LAI are unlikely to be in error more than ± 15%, and so sensitivity analysis suggests that resulting prediction errors

are, at most, ± 10% for GPP and ± 5% for LE fluxes. There was also sensitivity to reduced rooting depth; cutting rooting depth to 0.5 m from 1.5 m reduced both GPP and LE fluxes by over 30%. But increasing rooting depth by 25% increased both GPP and LE fluxes by only 1%; there was little sensitivity to increased rooting depth.

Plant processes were also sensitive to changes in total root biomass (Figures 6b and 6e). Halving root biomass cut annual GPP by 7% and LE fluxes by 16%, whereas a doubling increased production by 2% and evapotranspiration by 6%. The analyses indicated little sensitivity to more than a doubling in root biomass. In response to changes in root hydraulic resistivity, LE fluxes were more sensitive than photosynthesis. Cutting resistivity by 75% increased GPP and LE by 3 and 8%, respectively. Doubling resistivity reduced GPP by 3% and LE flux by 7%. Reducing plant conductivity by 50% cut GPP by 8% and LE fluxes by 14%, whereas a 50% increase in conductivity raised GPP and LE by 3 and 6%, respectively. Like root biomass, there was more sensitivity to reductions in conductivity than to increases in conductivity.

We found a relatively strong sensitivity to changes in minimum leaf water potential (Figures 6c and 6f). A 25% reduction cut production by 6% and evapotranspiration by 12%, whereas an increase of 25% raised production by 4% and evapotranspiration by 8%. The minimum leaf water potential has been relatively well defined by field measurements. Therefore, it is unlikely that the estimate used in the simulations (Table 2) is more than 10% in error, limiting prediction errors to ± 2% in GPP and ± 5% in LE fluxes. Fluxes were surprisingly insensitive to large changes in precipitation (Figures 6c and 6f). The analysis did not change the timing of precipitation, only the amount received. A 50% reduction in precipitation reduced GPP by < 4%, and reduced LE fluxes by 10%.

We examined how changes in soil texture (reduced content of sand) affected carbon and water interactions; textural changes affect the soil porosity, water retention curve and soil hydraulic conductivity (Saxton et al. 1986). With sand content reduced from 73% to 40%, the altered soil water retention curve had only minor effects on both GPP (+1%) and LE fluxes (+0.5%). We substituted a soil water retention curve derived empirically using TDR and predawn leaf water potential data obtained at the site, for that derived by Saxton et al. (1986). We found that, in 1996, using the relationships derived from local data had minor effects, increasing GPP by 2%, and LE fluxes by 1%.

Changes in root biomass at the soil surface, with total root biomass held constant, govern the uniformity of root distribution with depth. There were slight increases in GPP (+1%) and LE fluxes (+4%) when total root area was more evenly distributed with depth, by halving surface biomass. However, a doubling of surface biomass, with a concomitant decline in root biomass at depth, reduced both GPP (−3%) and LE fluxes (−8%). The LE fluxes were only slightly sensitive to large changes in through-fall fraction and in canopy surface storage capacity, and GPP was unaffected. Sensitivity to changes in the field capacity were steep, but relatively small (± 4%)
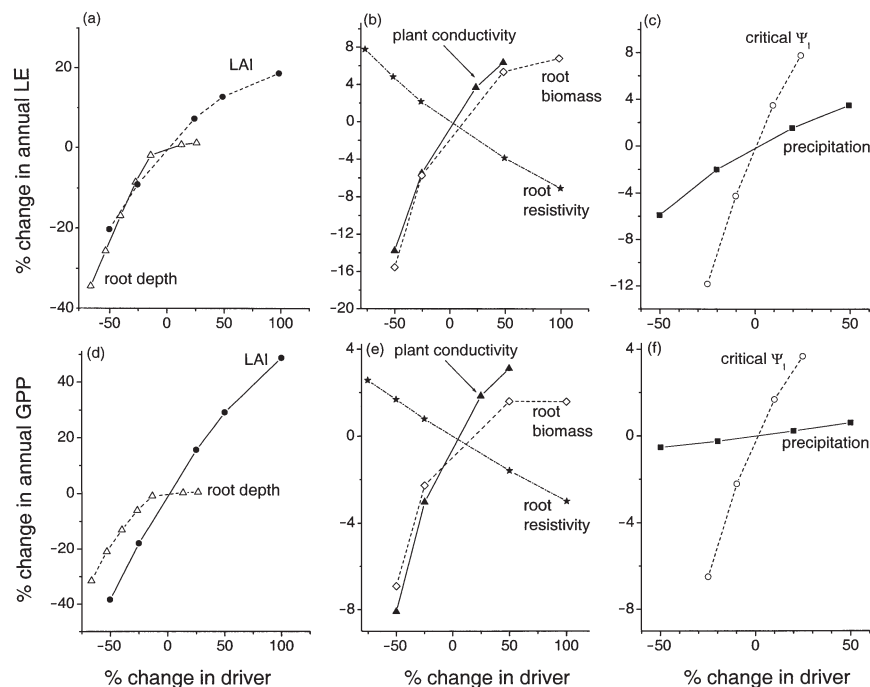
Figure 6. Analysis of the sensitivity of total annual latent energy (LE) fluxes (evapotranspiration and evaporation) (a–c) and annual gross primary production (GPP) (d–f) to changes in the values of seven key parameters. Axes show the percentage change in the parameters and predicted fluxes. For baseline parameter values see Table 2, and for baseline GPP and LE predictions see Table 1. Note the different scales on *y*-axes.

across the likely potential range of errors in parameter assignment (50 to 70% of total porosity). Both GPP and LE fluxes showed little sensitivity (< 2%) to large changes in root radius (–75% to +300%).

Discussion

There were important differences between the precipitation regimes in 1996 and 1997; the wet spring of 1996 was followed by a dry summer, whereas 1997 had less rain overall, but a more even distribution through the year. The total uptake of C and total transfer of water to the atmosphere were similar in both years (Table 1), according to both direct observation and simulations. Vegetation fluxes were virtually unaffected by major differences in the annual precipitation regime (Figure 5); simulations suggest that the allocation of roots below 1 m ensured that water was available through the extended summer drought of 1996 (Figure 4). With the same total root biomass but a rooting depth of only 0.7 m rather than 1.5 m, simulations indicate that both GPP and LE fluxes would have been reduced by > 20%, because of low summer recharge.

In both 1996 and 1997, there was a small decline in GPP predicted in late summer (Days 200–240), and some supporting evidence in the data. The model suggests that this decline was governed by two factors, the first related to atmospheric conditions and the second to soil characteristics. In the first case, on days with vapor pressure deficits > 3 kPa, atmospheric demand for water exceeded the supply capacity of the soil–plant hydraulic system. Stomatal conductance was reduced to restrict water losses, and productivity declined on these days. This stress was ephemeral and was relieved rapidly by the introduction of more humid air masses, as seen particu-

larly between Days 190 and 230 in 1996 (Figure 1). The second factor was related to the decline in soil water potential and soil hydraulic conductivity associated with drying soils, which reduced the maximum sustainable water flux, and thus stomatal conductance. The direct soil constraint developed slowly with the gradual drying of the soil profile, and was alleviated only by heavy autumn rains.

The sensitivity analyses served two purposes: they identified how alternate allocation patterns affect C and water interactions, and they quantified the relationships between parameter uncertainty and error propagation in model predictions. There were five parameters where intrinsic natural variability or uncertainty in parameter estimation were great enough to be associated with relatively large sensitivity in LE flux predictions: leaf area index, rooting depth, root biomass, plant hydraulic conductivity and root resistivity (Figures 6a and 6b). Of these five parameters, only two, leaf area index and rooting depth, were also linked to strong sensitivity in rates of primary production (Figures 6d and 6e). The relationship between LAI and irradiance exerts strong control over total water demand and production. Rooting depth is important to both C and water fluxes because it defines the plant's accessible soil volume, and thus determines whether water supply is vulnerable to periods of low recharge. Production was less sensitive to changes in the remaining three parameters; root biomass, plant conductivity and root resistivity. These parameters control the maximum rate of hydraulic flux through the soil–plant system. A reduction in the maximum flux reduced transpiration uniformly on days where demand exceeded supply. But, because photosynthesis was also limited by light absorption and foliar nutrient concentrations, depending on season, time of day or position in the canopy, reductions in C uptake were smaller

than reductions in water fluxes. The effect of shallow rooting is to cut production heavily once drought stress has developed, whereas the effect of parameters that reduce maximum hydraulic fluxes is to decrease production slightly during days of high atmospheric demand.

Maximum LAI in this ecosystem is low compared with other temperate forests (Aber 1979, Runyon et al. 1994), and yet production is sensitive to increases in LAI. Although allocation to foliage is relatively low, Law et al. (1999*b*) estimate the ratio of belowground C allocation to GPP is 0.61, and the ratio of belowground NPP to total NPP is 0.67, both very high ratios, and typical of vegetation with high water constraints. Although fire plays an important role in structuring ponderosa pine ecosystems (Monleon et al. 1997), simulations confirm that shallow-rooted vegetation will be severely drought-stressed in a summer resembling 1996. A shift in C allocation from below to above ground would boost production during periods when the soil profile was near field capacity (spring), but would also deplete soil water more rapidly through increased evapotranspiration in summer. Increased water use would induce more severe drought earlier in the summer, and if rooting depth was shallower, then vulnerability to severe drought would also rise.

The age structure of the stand indicates that recruitment is rare; there are only two major cohorts in the last 250 years. Seedlings and saplings are vulnerable to drought until their root mass and rooting depth develop. We have consistently observed mortality of young seedlings over the past several years following summer drought at the study site. Historical records suggest that the 45-year-old trees are the first successful cohort since fire suppression began in the area 100 years ago (S. Greene, US Forest Service, Corvallis, OR, unpublished data). Preliminary data on water stress in a nearby 15-year-old ponderosa pine stand compared with the old-growth site also support this theory (J. Irvine, Oregon State University, Corvallis, OR, unpublished data). A series of relatively wet summers may be required to allow tree maturation to the point where water below 0.5 m can be extracted by the roots. In *Pinus elliottii* Engelm. forests that experienced infrequent drought, the younger trees with more shallow root systems showed complete foliage loss, whereas a neighboring mature forest showed little sign of leaf mortality (H. Gholz, University of Florida, Gainesville, FL, unpublished data). This analysis suggests that an element of risk-avoidance needs to be incorporated in any hypothesis explaining allocation patterns; maintaining a large and active root system provides a buffer against life-threatening droughts. Climate variability may play an important role in setting optimal patterns of allocation above and below ground. A series of drought years occurring only intermittently may introduce stresses on forest development that constrain ecosystem dynamics and structure in important ways.

Effective modeling of carbon–water relations in this and other ecosystems is an important tool for scientific investigations, but is also increasingly important for ecosystem management and operational uses, such as predicting C storage and catchment hydrology under global change. In applying generic models to specific systems, it is critical to investigate the effects of parameter uncertainty, and the local applicability of empirically derived global algorithms. In this case, we examined the effect of using a generic soil water retention curve (Saxton et al. 1986) versus a curve developed empirically at the study site, and found insignificant differences in annual predictions. However, discrepancies between predicted and measured soil water content, especially during periods of recharge, suggest that the representation of macropore flow may be inadequate. We were also able to quantify the degree of error propagation from uncertainty in key parameters. The most sensitive parameter was LAI. Even in this intensively studied ecosystem, the difficulties in measuring LAI in an evergreen, needle-leafed open canopy forest introduce an uncertainty of ± 10% in GPP predictions.

The modeling did not take account of the highly heterogeneous nature of the site. A significant fraction of the soil or understory is exposed to direct radiation, whereas the foliage on larger stems is densely packed, so that locally, LAI can vary between 0 and 3. Larger stems are likely to dominate water extraction in the surrounding soils. Competition between trees for water may be important, and data quantifying the spatial allocation by individual trees to roots, both in the horizontal and the vertical planes, would be revealing. The critical importance of rooting depth, and the evidence that the majority of fixed C is allocated below ground, emphasize the need for more detailed studies on resource capture, both water and nutrients, in soils. This paper has demonstrated how, given measurements of ecosystem structure, reliable predictions of C and water exchange can be derived for a drought-stressed system. However, the longer term interaction between biology and environment that determines the ecosystem structure remains elusive, and should be the focus of future research.

References

Aber, J.D. 1979. Foliage-height profiles and succession in northern hardwood forests. Ecology 60:18–23.

Anthoni, P.M., B.E. Law and M.H. Unsworth. 1999. Carbon and water vapor exchange of an open-canopied ponderosa pine ecosystem. Agric. For. Meteorol. 95:115–168.

Choudhury, B.J. and J.L. Monteith. 1988. A four-layer model for the heat budget of homogeneous land surfaces. Quart. J. Roy. Met. Soc. 114:373–398.

Dawson, T.E. and J.S. Pate. 1996. Seasonal water uptake and movement in root systems of Australian phraeatophytic plants of dimorphic root morphology: a stable isotope investigation. Oecologia 107:13–20.

Eagleson, P.S. 1978. Climate, soil and vegetation. 1. Introduction to water balance dynamics. Water. Resour. Res. 14:705–712.

Epron, D., D. Godard, C. Cornic and B. Genty. 1995. Limitation of net CO_2 assimilation rate by internal resistances to CO_2 transfer in the leaves of two tree species (*Fagus sylvatica* L. and *Castanea sativa* Mill.). Plant Cell Environ. 18:43–52.

Farlow, S.J. 1993. Partial differential equations for scientists and engineers. Dover, New York, 414 p.

Foley, J.A., S. Levis, I.C. Prentice, D. Pollard and S.L. Thompson. 1998. Coupling dynamic models of climate and vegetation. Global Change Biol. 4:561–579.

Gash, J.H.C. 1979. An analytical model of rainfall interception by forests. Quart. J. Roy. Metereol. Soc. 105:43–55.

Hillel, D. 1980. Fundamentals of soil physics. Academic Press, Orlando, FL, 413 p.

Hillel, D. 1998. Environmental soil physics. Academic Press, San Diego, CA, 771 p.

Hinzman, L.D., D.J. Goering and D.L. Kane. 1998. A distributed thermal model for calculating soil temperature profiles and depth of thaw in permafrost regions. J. Geophys. Res. 103: 28,975–28,991.

Hodnett, M.G., L.P. da Silva, H.R. da Rocha and R.C. Senna. 1995. Seasonal soil water storage changes beneath central Amazonian rainforest and pasture. J. Hydrol. 170:233–254.

Houghton, J.T., L.G. Meira Filho, B.A. Callander, N. Harris, A. Kattenberg and K. Maskell. 1996. Climate change 1995, The science of climate change. Cambridge University Press, Cambridge, 572 p.

Law, B.E., D.D. Baldocchi and P.M. Anthoni. 1999*a*. Below-canopy and soil CO_2 fluxes in a ponderosa pine forest. Agric. For. Meteorol. 94:171–188.

Law, B.E., M.G. Ryan and P.M. Anthoni. 1999*b*. Seasonal and annual respiration of a ponderosa pine ecosystem. Global Change Biol. 5:169–182.

Law, B.E., R.H. Waring, P.M. Anthoni and J.D. Aber. 2000*a*. Measurements of gross and net ecosystem productivity and water vapour exchange of a *Pinus ponderosa* ecosystem, and an evaluation of two generalized models. Global Change Biol. 6:155–168.

Law, B.E., M. Williams, P.M. Anthoni, D.D. Baldocchi and M.H. Unsworth. 2000*b*. Measuring and modelling seasonal variation of carbon dioxide and water vapor exchange of a *Pinus ponderosa* forest subject to soil water deficit. Global Change Biol. 6: 613–630.

Melillo, J.M., J. Borchers, J. Chaney, H. Fisher, S. Fox and V. Members. 1995. Vegetation/ecosystem modeling and analysis project: comparing biogeography and biogeochemistry models in a continental-scale study of terrestrial ecosystem responses to climate change and CO_2 doubling. Global Biogeochem. Cycles 9: 407–437.

Monleon, V.J., K. Cromack and J. Landsberg. 1997. Short- and long-term effects of prescribed underburning on nitrogen availability in ponderosa pine stands in central Oregon. Can. J. For. Res. 27:369–378.

Newman, E.I. 1969. Resistance to water flow in soil and plant. I. Soil resistance in relation to amounts of root: theoretical estimates. J. Appl. Ecol. 6:1–12.

Press, W.H., B.P. Flannery, S.A. Teukolsky and W.T. Vetterling. 1986. Numerical recipes: the art of scientific computing. Cambridge University Press, Cambridge, 963 p.

Running, S.W. and J.C. Coughlan. 1988. A general model of forest ecosystem processes for regional applications. I. Hydrologic balance, canopy gas exchange and primary production processes. Ecol. Model. 42:125–154.

Runyon, J., R.H. Waring, S.N. Goward and J.M. Welles. 1994. Environmental limits on net primary production and light-use efficiency across the Oregon Transect. Ecol. Appl. 4:226–237.

Rutter, A.J., A.J. Morton and P.C. Robins. 1975. A predictive model of rainfall interception in forests. II. Generalization of the model and comparison with observations in some coniferous and hardwood stands. J. Appl. Ecol. 12:367–380.

Saxton, K.E., W.J. Rawls, J.S. Romberger and R.I. Papendick. 1986. Estimating generalized soil-water characteristics from texture. Soil. Sci. Soc. Am. J. 90:1031–1036.

Stephenson, N.L. 1990. Climatic control of vegetation distribution: the role of the water balance. Am. Nat. 135:649–670.

Tyree, M.T. and F.W. Ewers. 1996. Hydraulic architecture of woody tropical plants. *In* Tropical Forest Plant Ecophysiology. Eds. S.S. Mulkey, R.L. Chazdon and A.P. Smith. Chapman and Hall, New York, pp 217–243.

Waelbroeck, C. 1993. Climate–soil processes in the presence of permafrost; a systems modelling approach. Ecol. Model. 69:185–225.

Whitehead, D. 1998. Regulation of stomatal conductance and transpiration in forest canopies. Tree Physiol. 18:633–644.

Williams, M., E.B. Rastetter, D.N. Fernandes, M.L. Goulden, S.C. Wofsy, G.R. Shaver, J.M. Melillo, J.W. Munger, S.-M. Fan and K.J. Nadelhoffer. 1996. Modelling the soil–plant–atmosphere continuum in a *Quercus–Acer* stand at Harvard Forest: the regulation of stomatal conductance by light, nitrogen and soil/plant hydraulic properties. Plant Cell Environ. 19:911–927.

Williams, M., Y. Malhi, A. Nobre, E.B. Rastetter, J. Grace and M.G.P. Pereira. 1998. Seasonal variation in net carbon exchange and evapotranspiration in a Brazilian rain forest: a modelling analysis. Plant Cell Environ. 21:953–968.

Williams, M., W. Eugster, E.B. Rastetter, J.P. McFadden and F.S. Chapin, III. 2000. The controls on net ecosystem productivity along an arctic transect: a model comparison with flux measurements. Global Change Biol. 6 (Suppl.):116–126.

Woodward, F.I. 1987. Climate and plant distribution. Cambridge Univ. Press, Cambridge, 174 p.

Appendix: Soil surface energy balance

Sensible heat fluxes are determined from the temperature gradient between the soil surface (T_s, K) and the air above (T_a, K), and the specific heat capacity (c_p, J kg^{-1} K^{-1}), density (ρ_a, kg m^{-3}), and heat conductance (g_{AH}, m s^{-1}) of air,

$$Q_h = c_p \rho_a g_{AH}(T_a - T_{sur}). \tag{A1}$$

Latent heat flux is estimated from the latent heat of vaporization (λ, J kg^{-1}), vapor boundary layer conductance (g_{AW}, m s^{-1}), soil conductance to water vapor transfer (g_{ws}, m s^{-1}), atmospheric pressure (P_a, Pa), and the gradient of vapor pressure (e) between the soil air spaces (e_s, Pa) and the air above (e_a, Pa):

$$Q_e = \lambda \rho_a \frac{0.622(e_a - e_s)}{P_a(1/g_{AW} + 1/g_{ws})}. \tag{A2}$$

The vapor pressure in the soil air spaces (e_s, Pa) is deter-

mined from the saturation vapor pressure (e_{sat}, Pa) in the air spaces of the surface layer, the soil water potential (Ψ_s, Pa) of the surface layer, the partial molal volume of water (V_w, m^3 mol^{-1}), and the gas constant ($\Re$, Pa m^3 mol^{-1} K^{-1}):

$$e_s = e_{sat} \exp\left(\frac{\Psi_s \overline{V}_w}{\Re T_s}\right). \tag{A3}$$

Following Choudhury and Monteith (1988), g_{ws} is dependent on the diffusion coefficient of water vapor in air (D_w, m^2 s^{-1}), the tortuosity (τ) and porosity (ζ) of the soil surface layers (determined by the physical structure of the soil matrix), and the thickness of the dry soil at the surface (l_t). Porosity is determined as the portion of soil volume that is not occupied by mineral, organic and water fractions. Thus,

$$g_{ws} = \zeta D_w / (\tau l_t). \tag{A4}$$

We assume that the distance from the soil surface to the top of the wetted soil layer (which is equal to l_t) is increased by soil evaporation, and reduced by dew formation and precipitation (I, mm), while the total water content of the surface layer is also altered by root water uptake and gravitational drainage. We calculate the magnitude of wetting or drying (Δl, mm):

$$\Delta l = -(\Delta t Q_e / \lambda + I)\theta_f, \tag{A5}$$

where θ_f is the field capacity and Δt is the time-step length (s). Drying ($\Delta l > 0$) increases the distance to the top of the wetted soil (l_t):

$$\text{If } \Delta l > 0,\ l_t = l_t + \Delta l. \tag{A6}$$

Wetting can have two effects. If the wetting depth Δl is less than the thickness of the current surface dry layer, then a new wet layer (here denoted *) is formed, extending from close to the surface ($l_{t*} = l_{min}$, the minimum wetting depth) to a depth l_{b*}:

$$\text{If } \Delta l < l_t,\ l_{t*} = l_{min},\ l_{b*} = \Delta l, \tag{A7}$$

thus sandwiching a dry layer, extending from l_{b*} to l_t, between two wet layers.

Alternatively, the wetting recharges the current wet layer, filling it first to the surface, with remaining water extending its depth, l_b:

$$\text{If } \Delta l > l_t,\ l_t = l_{min},\ l_b = l_b + (l_t - \Delta l). \tag{A8}$$

The distance from the soil surface to the topmost wetted layer determines l_t for the soil evaporation equation.

Atmospheric conductance to heat and water vapor are assumed equal and are dependent on wind-speed (u_z, m s^{-1}, where z is measurement height), the von Karman constant (0.41), and mean surface roughness (z_o, m), here set at 13% of canopy height:

$$g_{AH} = g_{AW} = \frac{u_z k^2}{[\ln(z/z_o)]^2}. \tag{A9}$$